A Polycaprolactone-Based Compatibilization Treatment to Improve Dispersion and Interphase Structure of Silica Polyurethane Composites

Leonel Matias Chiacchiarelli,[1] Leandro Monsalve,[2] Analía Vázquez,[2] José M. Kenny,[1,3] Luigi Torre[1]
[1] *Department of Civil and Environmental Engineering, University of Perugia, UdR INSTM, Strada di Pentima 4, 05100 Terni, Italy*

[2] *Polymer and Composite Material Group, INTECIN-CONICET, Construction Department, Engineering Faculty, Universidad de Buenos Aires, Las Heras 2214, 1127AAR, Buenos Aires, Argentina*

[3] *Institute of Polymer Science and Technology, CSIC, Juan de la Cierva 3, 28006 Madrid, Spain*

Silica nanoparticles (SNs) were grafted with ε-caprolactone using an environmentally friendly approach. By using tartaric acid as a catalyst and the silanol groups as initiators, grafted nanoparticles (GNs) with organic weight fractions (w_{of}) within the range 0–46 wt% were synthesized. Thermogravimetric (TGA) and infrared analysis were used to measure the w_{of} and to corroborate the covalent bond between the SN and the caprolactone monomer. Transmission electron micrographs of the polyurethane (PU) nanocomposites based on the SN and the GN revealed that the interfacial area of the GN-based PU increased by the reduction of agglomerate dimensions from 10 μm to around 0.1 μm. Dynamic mechanical analysis showed that the GN nanocomposites improved the storage shear modulus from 616±11 to 849±8 MPa for a GN with w_{of} = 16.7% and 3 wt% filler concentration. In addition, the GN particles prevented a relevant decrease of the transition temperature (T_g). Differential scanning calorimetry corroborated that GN increased the enthalpic energy associated to the physical crosslinking of the hard segments (HS). Wide-angle X-ray diffraction proved that the GN formed a HS structure with improved crystallinity. The thermal stability of the GN-based PU a nanocomposite was improved by an increase of the thermal stability of the castor oil soft segments. POLYM. ENG. SCI., 00:000–000, 2013. © 2013 Society of Plastics Engineers

INTRODUCTION

The development of composites with fillers which have at least one physical dimension in the nanometer scale is governed by interface compatibility aspects [1, 2]. Because of the frequent use of inorganic nanoparticles, its dispersion within the organic matrix represents the biggest challenge toward the development of composites with improved properties. An inadequate dispersion of the inorganic filler in the organic matrix could produce a substantial deterioration of properties, rendering the use of the fillers inappropriate [3]. In addition, in order to fully exploit the properties of the filler, it is generally accepted that the interphase area between the matrix and the filler should be maximized. Under these circumstances, even at low filler concentrations (~1 wt%), substantial mechanical improvements can be obtained. To achieve this, several compatibilization methods have been studied [4–7]. The most relevant aspect it is to generate an interphase which is highly compatible with both the matrix and the filler. This improves compatibility, dispersibility and produces a stress-transfer effect between the filler and the matrix. One method that has been studied extensively in literature is the "grafting-from" technique [8–12]. By using the free radicals on the surface of the filler as initiators, polymeric molecules can be growth with a high grafting density. With this approach, the free radical left after the growth process can be covalently bonded to the matrix, obtaining an effective stress-transfer effect. In addition, the organic layer which covers the inorganic particle forms a core–shell-type structure [13], which constitutes an optimized interphase between the inorganic filler and the organic polymer matrix. Even though this grafting technique has been proposed by several authors as the most advantageous [11], the frequent use of heavy metal-based catalysts during the synthesis [10, 14, 15] might impose an important drawback toward the development of an environmentally friendly approach.

Silica is one of the most employed additives in the polymer industry [8, 16]. Typically, several compatibilization

Correspondence to: Luigi Torre; e-mail: torrel@unipg.it
DOI 10.1002/pen.23723
Published online in Wiley Online Library (wileyonlinelibrary.com).

methods are implemented for its specific application. The vast majority of those methods are based on the use of heavy metal-based catalysts or other toxic chemical precursors. Dubois et al. [13] used toluene diisocyanate as an agent to compatibilize the surface of silica nanoparticles (SNs) in order to improve the matrix-filler compatibility. They were able to control and design the interphase, improving substantially compatibility, and obtaining polyurethane (PU) composites with improved mechanical properties. Another compatibilization method is based on silane-coupling agents, such as aminopropyltriethoxysilane (APTS) [8]. Its application to improve the interphase properties of PU composites has already been studied extensively [17–19]. Other compatibilization methods are based on the use of biodegradable polymers, such as polycaprolactone (PCL). Joubert [14, 20] implemented a grafting from technique which covered the outer surface of silica particles with PCL. They were able to obtain a high grafting density and an improved compatibility with PCL-based composites. However, the compatibilization treatment was based on the use of heavy metal catalysts. The reinforcement of a PU matrix with graphene nanofillers has been studied by Lee et al. [5], Nguyen et al. [6], and Raghu et al.[7]. To achieve graphene exfoliation, an oxidation functionalization method was performed. Hence, the graphene-based nanocomposites showed improved conductivity and mechanical properties. However, the main limitation was associated to the functionalization method, which was based on the use of corrosive acids.

Several publications have dealt with the development of silica PU nanocomposites [3, 13, 17, 21–31]. Petrovic et al. [28, 32] studied the effect of SN on the segmented structure of PUs. X-ray diffraction (XRD) analysis revealed that the addition of SN deteriorated the crystallinity of the HS. Even though the mechanical properties were improved by the addition of a harder silica phase, those were simultaneously deteriorated by the reduction of the physical crosslinking within the HS. Lee et al. [33] studied the dispersion of SN in a PU matrix. Even though a nanocomposite at 3 wt% showed improved elasticity, the dispersion of the SN in the PU matrix revealed that the interfacial area between the filler and the matrix was deteriorated by the conglomeration of the SN into elongated shapes. The reinforcement of castor oil-based PU with nanoparticles has been studied by several researchers [34–42]. The mechanical properties of nanocomposites reinforced with nanocellulose, banana fibers, Titanium Dioxide, clay and other nanoparticles have been evaluated. However, as far as the author is concerned, the use of SN has not been studied extensively. Varma et al. [37] found that the compatibility between the silica filler and the castor oil-based PU matrix was poor. Hence, the nanocomposites did not improve significantly the mechanical performance of the PU matrix. Xia et al. [38] studied the reinforcement of waterborne PUs with SN prepared with a sol–gel method. Even though the method proved to form nanocomposites with improved tensile and thermal properties, the synthesis was performed by the use of toxic compounds, such as APTS.

In this work, in contrast to what has been done in literature, the authors implement a simplified and environmentally friendly compatibilization treatment for the development of grafted silica PU nanocomposites. The main novelty is the synthesis of PCL-grafted SNs using an organic acid as a catalyst instead of the traditional heavy metal-based catalyst. This approach rendered the compatibilization treatment innocuous. The resulting grafted nanoparticle (GN) consisted of bio-based shell that covered the inorganic silica core. This grafted silica was subsequently inserted in a bio-based PU matrix. The filler dispersion, thermal properties, and dynamic mechanical properties were evaluated as a function of the organic weight fraction of the nanoparticle and its concentration.

MATERIALS AND METHODS

Tartaric acid (ACS reagent), ε-caprolactone (97%), and toluene (anhydrous, 99.8%) were purchased from Sigma-Aldrich and used without further purification. Hydrophilic silica (Aerosil® A300) was purchased from Degussa. The nanoparticles had an average diameter of 7 nm and a specific surface area of 300 m^2/g. In order to remove the humidity accumulated by storage, the silica was dried in a vacuum furnace (110°C, 40 mbar, overnight) before use. As far as the PU formulation is concerned, the isocyanate component was kindly supplied by Chimicafine S.R.L. (Suprasec® 2214). It was a low viscosity (30 mPa.s at room temperature) diphenyl methane diisocyanate with an isocyanate (NCO) value of 32%. The polyol component was kindly supplied by Neuchem (Albodur® 941). It was a bio-based polyol (produced from castor-oil) with a viscosity of 300 mPa.s at room temperature and an OH number of 318 $mgKOHg^{-1}$. Both components were dried in a vacuum mixer before use (Dispermat LC30). This process was performed at 1000 rpm in a 40 mbar vacuum for 1 hr.

Differential scanning calorimetry (DSC) analysis was performed using a TA instruments Q200. The samples were tested using a full thermal cycle which consisted on three stages. In the first one, the sample was heated from −80°C up to 100°C at a heating rate of 5°C min^{-1}. The second one consisted on cooling the sample from 100°C down to −80°C at a cooling rate of 5°C min^{-1}. Finally, the last stage was identical to the first one. The reproducibility was tested by measuring at least three samples. Thermogravimetric analysis (TGA) was performed using a Seiko Exstar 6300. The samples were tested in a nitrogen atmosphere using a thermal cycle which started at 30°C and went up to 800°C at a heating rate of 15°C min^{-1}. The reproducibility was tested by measuring at least three samples. Dynamic mechanical analysis (DMA) analysis was performed using an Ares N2 Rheometer in the torsion mode. The experiments were done using a temperature ramp from 30°C up to 120°C with a rate of 20°C min^{-1}. In addition, the frequency was set to 1 Hz and the strain to

 DOI 10.1002/pen

0.1. Fourier transform infrared analysis (FTIR) was performed with a Shimadzu Affinity spectrometer using the transmission method. To achieve this, the samples were mixed with KBr powder and subsequently pressed to pellet morphology. Transmission electron micrograph (TEM) analysis of the cured composite was done using a Philips EM-208 system. XRD spectra were measured with a Bruker D8 Advance operated by a CuKα with a $\lambda = 1.54$ Å. The data collection was recorded with a Vantec detector in the range $2\Theta = 2$–$50°$. The scan rate was set to 0.5 sec per step and 0.024° per step. A commercial Peak Fitting Module (Microlocal OriginPro 8.0) was used for the Gaussian decomposition of the diffraction patterns.

The synthesis of the grafted silica was performed following a modified process based on the work of Casas [10]. A typical reaction consisted of mixing toluene and silica in a round flask using an ultrasonic mixer for 30′ (Testlab TB02TA). Afterward, the round flask was introduced on top of a heating-stirring plate (Velp Scientific). The temperature was increased to a value higher than the boiling temperature of the solvent (120°C) and the exit of the round flask was connected to a Dean-Stark trap and in series with a water-cooled condenser. This system permitted the recirculation of toluene (evaporation–condensation) with a simultaneous decrease in humidity, avoiding the use of a nitrogen purge. In addition, the reaction temperature was fixed to the boiling temperature of the solvent (111°C). The silica-solvent mixture was then continually mechanically stirred and the tartaric acid catalyst was added through a side compartment of the round flask. Finally, the specific amount of ε-caprolactone was added and the reaction continued for a reaction time of 24 hr. When the reaction was finished, the grafted silica was separated from the solvent with centrifugation. For each centrifugation step (10,000 rpm for 10 min), toluene was added and mixed so as to remove any unreacted component. Finally, the grafted silica was heat treated at 80°C in a vacuum furnace for 24 hr. It is important to emphasize that, during the reaction, the reactive mixture was constantly stirred at a substantial rotation rate (600 rpm). This is an essential aspect so as to avoid silica aggregation and a subsequent effect in the grafting kinetics [43]. It should be noticed that there are several ways to describe how the grafting process covers the silica surface [9–11, 14, 20, 44–46]; however, in this work we will use the organic weight fraction of the GN as the main parameter. This is obtained using TGA analysis, where it is possible to discern the inorganic (silica) and organic (grafted caprolactone) weight fractions. Hence, the organic weight fraction is defined as,

$$w_{of} = \frac{w_{organic}}{w_{inorganic+organic}} \tag{1}$$

even though it is possible to a priori select the organic weight fraction of the final GN, the range of w_{of} used in this work was within 10–46%. The quantitative values of the precursors to obtain low (<20%) and high (>40%) w_{of} are reported in Table 1.

The preparation of the Sil-PU composite compromised a series of steps. Initially, the grafted silica powder was mixed with the polyol component using an Ultra Turrax device (IKA T18) for 10 min at 10,000 rpm. This initial step was essential to reduce the size of the tactoids formed after the synthesis of the grafted silica. Afterward, the mixture was further mixed in a high shear-mixing unit (Dispermat LC30). This device was able to control both temperature and vacuum in addition to rotation speed. Hence, the mixture was dispersed at 10,000 rpm maintaining a vacuum of 40 mbar and a constant temperature of 30°C. Special attention was taken so as to form and maintain the doughnut effect [47]. Afterward, the isocyanate component was added and further mixed at 1000 rpm under vacuum (40 mbar). The isocyanate/polyol weight ratio was calculated using an index of 1.05. Finally, the reactive mixture was poured onto the surface of a dried Teflon mold. The cure process consisted in two steps: an initial one at 25°C for 24 hr and a subsequent one at 60°C for 72 hr.

The micrographic information presented in this work was based on the observation of at least three micrographs at several magnifications (×11,000, ×110,000 and ×180,000). Those magnifications were chosen because it was possible to distinguish the agglomerate dimensions and the distances between the nanoparticles. The dispersion of the nanoparticles in the PU matrix was qualitatively characterized using the concepts of agglomerate size and the interparticle distance. An agglomerate was referred specifically to an irregular distribution of SNs that can be distinguished in the micrometer scale. For this reason, low-magnification micrographs were particularly useful to qualitative evaluate the dimensions of those agglomerates. In contrast, the interparticle distance was referred to the distance between the spherical nanoparticles (within an agglomerate).

In this work, the pristine SN will be referred as SN. Instead, the grafted silica will be referred as GN. The general denomination of the PU nanocomposites was Sil(X%)-PU Y wt%, where X represented the organic weight fraction percent of the GN and Y represented the filler concentration of the PU nanocomposite. The PU

TABLE 1. Quantitative values of the reactions.

	Toluene (ml)	Silica (g)	Caprolactone (ml)	Tartaric acid (mg)	Reaction time	Temperature (°C)
Low grafting	100	1	2	28.4	24	111
High	100	1	12	28.4	24	111

matrix was denominated as Neat-PU. The hard segments (HS) were associated to the isocyanate precursor while the soft segments (SS) were associated to the castor oil-based polyol.

RESULTS AND DISCUSSION

Grafted Nanoparticle Characterization

TGA analysis was used to determine the weight fraction of grafted caprolactone on the SN (w_{of}). The weight loss (WL) of the GN as a function of temperature and w_{of} is shown in Fig. 1. It should be noticed that, in this temperature range, the SN showed a WL which was less than 2 wt%. Hence, its representation in Fig. 1 was omitted. The GN had a substantial WL centered at a temperature of 427°C. Even though the main WL associated to the degradation of the organic part of the nanoparticle was centered at that temperature, from the results it can be inferred that organic degradation also occurred in the temperature range 250–550°C. In contrast, the WL after 600°C was negligible. Due to the fact that the WL measured in the temperature range 250–550°C was associated to the degradation of the organic content of the grafted silica, the organic weight fraction can be calculated using the following equation,

$$w_{of} = \frac{w_{550\,^\circ C} - w_{25\,^\circ C}}{w_{25\,^\circ C}} \tag{2}$$

then, from Fig. 1, it can be calculated that the GNs had an organic content of 28.9 and 46.2% wt, respectively. These results proved to be in agreement with previous publications [44]. Hence, the main degradation centered at 427°C can be associated to the degradation of a hypothetical PCL molecule with an average molecular weight of 1032 and 1516 g mol^{-1}, for w_{of}=28.9% and w_{of}=46.2%, respectively. The calculations of the molecular weight were based on the assumption that the growth mechanism followed a "living" mechanism [10]. The WL that was also present in adjacent temperatures (250–350°C and 450–550°C) can be associated to the fact that the polydispersity index of the synthesis process was not equal to 1 [10].

The FTIR spectra of the SN and GN used in this work are shown in Fig. 2. In particular, the spectra of the SN and two different GN (with w_{of} = 28.9% and w_{of} = 46.2%) are depicted. The main visible infrared absorption is related to the vibration mode of the Si-O-Si molecule, which absorbs over a broad wavelength centered at ~1100 cm^{-1} [24, 43]. The area of the absorption versus wavelength spectra can be directly correlated to the amount of inorganic material present on the nanoparticle. This absorption mode is present in all of the spectra presented because the grafting did not alter the amount of inorganic material of the nanoparticle. An additional infrared absorption related to the stretching mode of the O—H group of both water and silanol is centered at an approximate wavelength of 3450 cm^{-1}. The fact that this mode was only active on the SN spectra indicated that the grafting process was successful. An additional infrared absorption related to the stretching mode of the carbonyl group (C═O) was centered at a wavelength of ~1735 cm^{-1}. In addition, an absorption mode of alkane type group (C—H) was also measured in a wavelength centered at round 2925 cm^{-1}. These last modes were directly related to the organic part of the GNs and a further indication of the successful ring-opening polymerization from the ε-caprolactone precursor [48, 49].

Filler Dispersion in the PU Matrix

The dispersion of the filler in the PU matrix was studied as a function of filler concentration and w_{of}. The

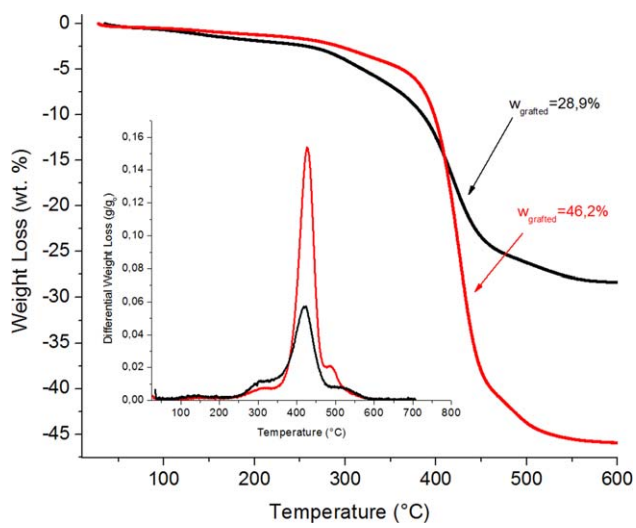

FIG. 1. Thermogravimetric weight loss of GN with w_{of} = 28.9% and w_{of} = 46.2%. [Color figure can be viewed in the online issue, which is available at wileyonlinelibrary.com.]

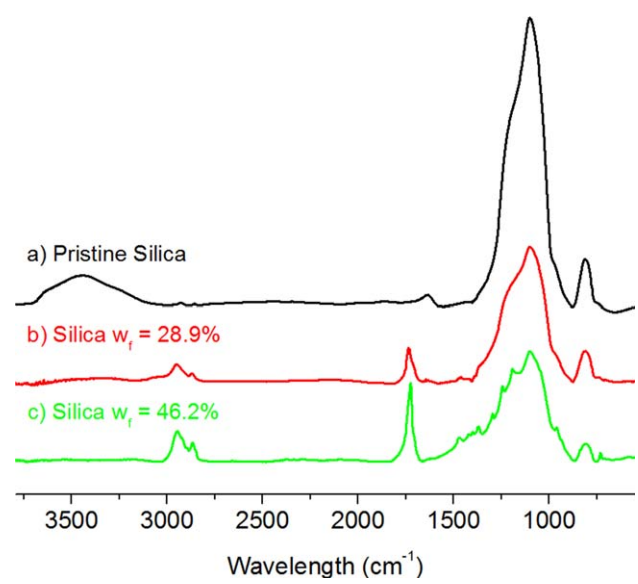

FIG. 2. Absorption infrared spectra of (a) SN, (b) GN with w_{of} = 28.9%, and (c) GN with w_{of}=46.2%. [Color figure can be viewed in the online issue, which is available at wileyonlinelibrary.com.]

 DOI 10.1002/pen

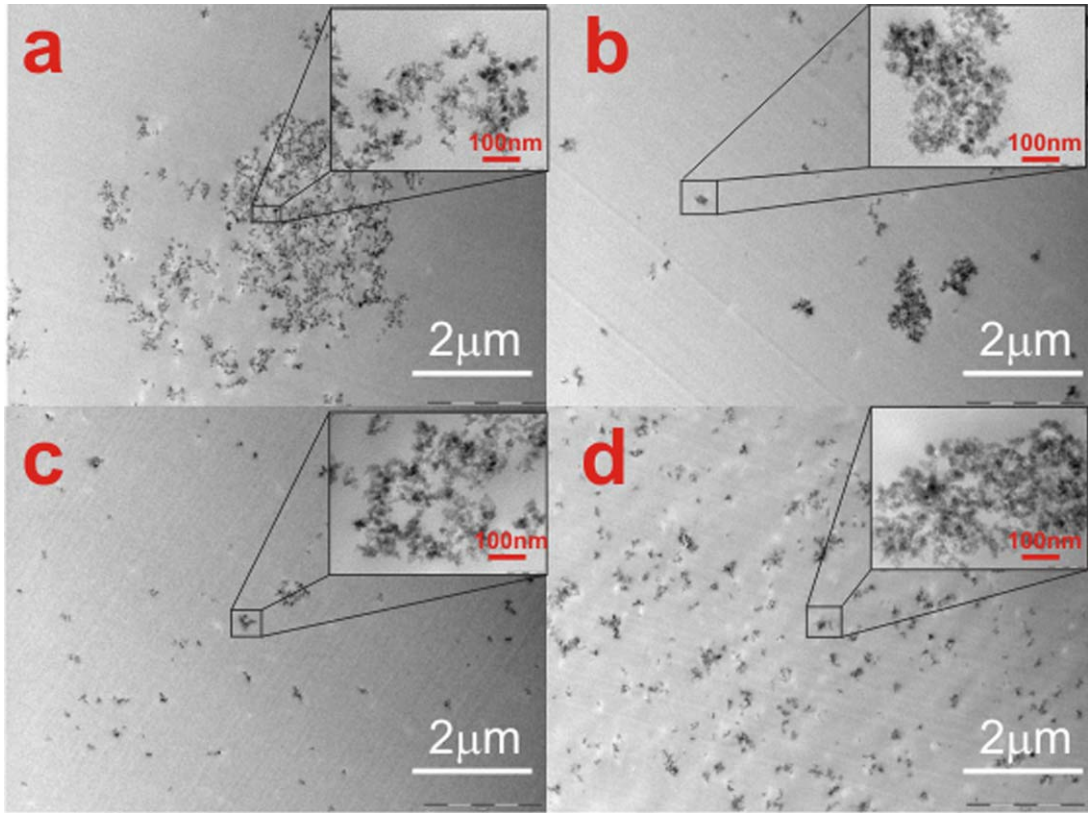

FIG. 3. TEM micrographs showing the dispersion of (a) Sil-PU 1 wt%, (b) Sil(13%)-PU 1 wt%, (c) Sil(24%)-PU 1 wt%, and (d) Sil(25%)-PU 3 wt%. [Color figure can be viewed in the online issue, which is available at wileyonlinelibrary.com.]

TEM micrographs showing the effect of the previously mentioned variables are shown in Fig. 3. For the case of the SN (Fig. 3a), the micrographs at low magnification showed a strong tendency to form agglomerates of very heterogeneous dimensions (within the range 0.1–10 μm). The analysis at high magnifications (inset Fig. 3a) revealed that the interparticle distances were small and the nanoparticles were arranged in clusters with a spiral shape. These features are in agreement with other publications that studied the dispersion of these types of nanocomposites [8, 17, 19, 21, 23, 24, 28, 32, 50, 51]. The main reason for the formation of those elongated shapes was related to hydrogen type interactions among each SN. Taking into account the elevated density of silanol groups [43], a strong interaction was expected. This interaction was the main cause for the formation of agglomerates. In addition, as it can be noticed in Fig. 3a, the dispersion process was able to substantially deform the initial agglomerated structure, but it was unable to breakdown the agglomerates into isolated nanoparticles.

In contrast, the dispersion analysis of the GN in a Sil(13%)-PU 1 wt % is shown in Fig. 3b. At low magnifications, the agglomerates were not arranged in spiral shapes. The agglomerate size was found to be in the order of 0.1μm and with a much reduced dimensional heterogeneity. At high magnifications (inset of Fig. 3b), the interparticle distances were similar to the SN dispersion (inset of Fig. 3a). Then, GN with $w_{of} = 13\%$ increased substantially the interfacial area between matrix and filler by the reduction of agglomerate dimensions (up to two orders of magnitude). This result can be understood by considering that the grafting process inhibited hydrogen interactions through the reduction of the silanol surface density. Those interactions were responsible for the conglomeration of the SN into elongated shapes.

To further evaluate the grafting effect on dispersion, the analysis of a nanocomposite with nanoparticles grafted with $w_{of} = 23\%$ is shown in Fig. 3c. At low magnifications, the micrographs clearly show that the agglomerate dimensions were furtherly reduced. In contrast, at higher magnifications (inset of Fig. 3c), the interparticle distances remained almost unchanged (similar to what has been found at $w_{of} = 13\%$). Taking into account that a higher w_{of} further reduced the particle silanol surface density, then, it can be inferred that this result corroborates that the mechanism responsible for the formation of agglomerates was related to hydrogen type interactions.

The effect of increasing filler concentration on the dispersion of a GN is shown in Fig. 3c and d. The micrographs illustrate how the agglomerate dimensions and interparticle distances changed when the concentration of the filler increased from 1 to 3 wt%, maintaining a similar w_{of}. At low magnifications, it was possible to discern that the agglomerates dimensions increased as a function

of increasing concentration. At high magnifications (inset of Fig. 3d), the discernible interparticle distances did not change substantially as a function of increasing filler concentration. Hence, it can be concluded that the dispersion was deteriorated as a function of increasing concentration, mainly by the formation of bigger agglomerates but without a discernible change of interparticle distances. However, the interfacial area remained high enough to consider that the composite was reinforced by a nanometric structured filler.

Thermal Properties

The thermal stability of the PU nanocomposites was evaluated with TGA. The weight residue (WR) as a function of temperature is shown in Fig. 4. For the case of the Neat-PU, the thermal degradation was characterized by two stages. In the first one, which was centered at a temperature of 330°C, the thermal degradation was associated to the decomposition of the HS. The second stage, which was centered at a temperature of ~470°C, was associated to the decomposition of the SS. The WR at 600°C was 5.17%. The results found in this work are in agreement with previous studies of thermal degradation of castor oil-based PUs [52–54]. The thermal degradation of Sil-PU at 1 and 3 wt% showed that the SN did not modify at all the thermal stability of the Neat-PU matrix. The measured WR at 600°C were 5.96 and 8.41% for filler concentrations of 1 and 3 wt%, respectively. This indicated that the HS and the SS were thermally degraded whereas the SN did not. This result was expected because the onset of degradation of the SN was above 800°C [43]. In contrast, the GN-based nanocomposites have shown to improve the thermal stability of the Neat-PU. Even though the HS degradation stage remained practically unchanged, the thermal degradation of the SS stage was improved. For a filler concentration of 1 wt% and a w_{of} of 13%, the thermal degradation of the SS was substantially improved. At 550°C, the WR increased from ~5% to around 20%. Hence, it can be concluded that nanocomposites based on GN improved thermal stability while nanocomposites based on SN did not.

The thermal transitions of the PU samples were analyzed with DSC as a function of w_{of} and filler concentration. Taking into account the structure of the Neat-PU, two main transitions associated to the SS and the HS were expected. The effect of the w_{of} and filler concentration on the HS thermal transition is shown in Fig. 5. For the Neat-PU (Fig. 5a), both the first heating cycle and the subsequent one were depicted. On the first heating cycle, a wide endothermic transition centered at a $T = 60$°C was found. The complex shape of the transition has already been studied extensively [55–58]. It is not the objective of this work to discuss the details of that transition but, rather, to emphasize that the HS were arranged in an ordered structure which was destroyed after the temperature went above 60°C. The enthalpy associated to that transition was 0.59 J/g. The ordered structure was composed of HS interconnected with hydrogen type interactions, forming what is known as physical crosslinking [59, 60]. It should be noted that the ordered HS structure of the Neat-PU was expected because the postcure cycle was designed with that purpose. An additional fact which correlated the formation of the ordered structure with the postcure of the Neat-PU was found in the second DSC heating cycle (Fig. 5a), where the enthalpic transition was absent.

In contrast, when the Neat-PU was modified by the addition of 1 wt% of SN (Fig. 5b), the shape of the transition was substantially altered. Specifically, the enthalpic energy associated to the transition was reduced to

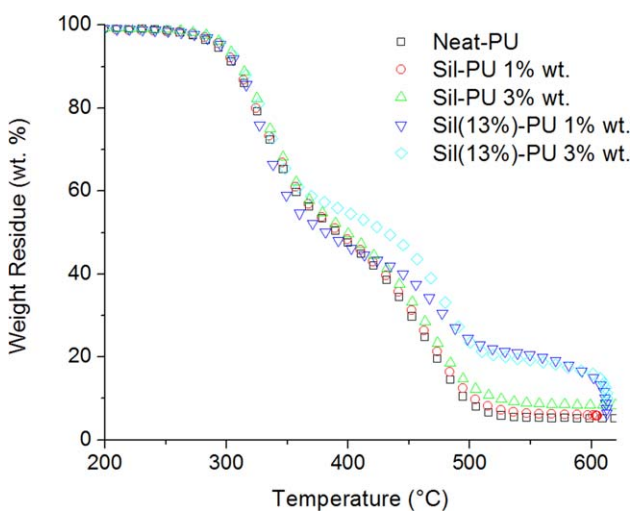

FIG. 4. Weight residue as a function of temperature for the Neat-PU, Sil-PU 1, and 3 wt%, Sil(13%)-PU 1 wt%, and the Sil(13%)-PU 3 wt %. [Color figure can be viewed in the online issue, which is available at wileyonlinelibrary.com.]

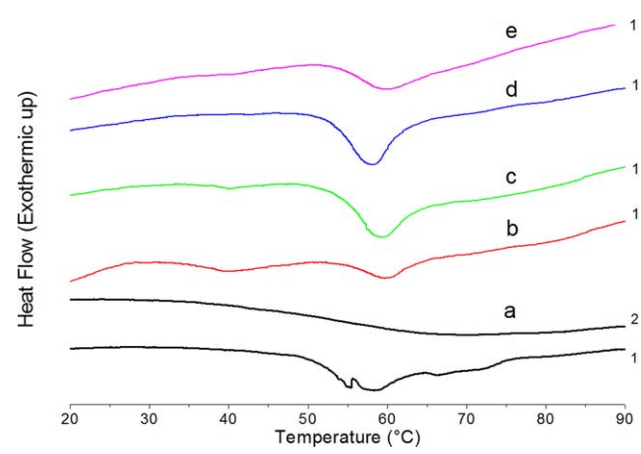

FIG. 5. Heat flow (exothermic up) as a function of temperature for (a) Neat-PU, (b) Sil-PU 1 wt%, (c) Sil(13%)-PU 1 wt%, (d) Sil(29%)-PU 1 wt%, and (e) Sil(13%)-PU 3 wt%. The numbers on the right of the diagram specify the heating cycle stage. [Color figure can be viewed in the online issue, which is available at wileyonlinelibrary.com.]

 DOI 10.1002/pen

0.099 J/g. Hence, it can be deduced that comparing the HS structure of the Neat-PU and the Sil-PU, the physical crosslinking in the Sil-PU was substantially reduced. It should be noted that several researchers [8, 32, 61] have already found that the SN were the cause of the destruction of the ordered HS structure.

A completely different scenario was found for the case of the nanocomposites prepared with GN (Fig. 5c–e). For example, comparing the thermal transitions of the Sil-PU 1 wt% and the Sil(13%)-PU 1 wt%, which are depicted in Fig. 5b and c, it can be deduced that the grafting process promoted the ordering of the HS. The enthalpic contribution increased from 0.099 to 0.19 J/g. In addition, by fixing filler concentration and increasing w_{of}, the same tendency was found. As depicted in Fig. 5c and d, an increase of w_{of} from 13 to 29% increased the enthalpy from 0.19 to 0.52 J/g. Finally, an increase in filler concentration from 1 to 3 wt% caused a significant broadening of the enthalpic transition, furtherly increasing the enthalpic contribution from 0.52 to 0.71 J/g. Then, it can be concluded that the grafting process was able to improve the compatibility with the PU matrix by promoting the physical crosslinking within the HS.

The effect of the w_{of} and filler concentration on the thermal transition of the SS is shown in Fig. 6. For the Neat-PU (Fig. 6a), two transitions centered at −7.8 and 8.9°C were found. It should be emphasized that the chemical composition of the castor oil polyol used in this work was very heterogeneous, then, a series of transitions were expected. In contrast to synthetic polyols, castor oil-based polyols present a more complex behavior [52–54]. The Sil-PU 1 wt% nanocomposite showed only one weak transition centered at a temperature of approximately −7.2°C. The effect of w_{of} and filler concentration was not relevant, changing the amount of transitions but to a much lesser extent. Hence, it can be concluded that the SS transition was not substantially modified by the grafting process.

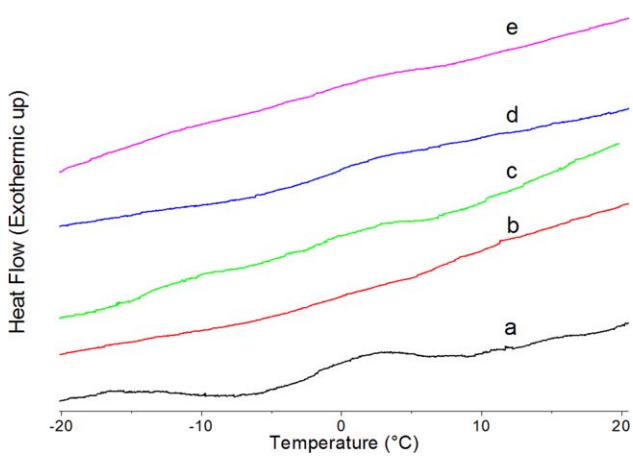

FIG. 6. Heat flow (Exothermic up) as a function of temperature for (a) Neat-PU, (b) Sil-PU 1 wt%, (c) Sil(13%)-PU 1 wt%, (d) Sil(29%)-PU 1 wt%, and (e) Sil(13%)-PU 3 wt%. [Color figure can be viewed in the online issue, which is available at wileyonlinelibrary.com.]

Dynamical Mechanical Analysis

The DMA behavior of the nanocomposites developed in this work was studied as a function of w_{of} and filler concentration. Similar to the DSC experiments, it was expected to have two transitions. The first one was related to the softening of the SS, which is usually found at temperatures which are lower than room temperature. This transition is of fundamental importance for the low temperature behavior of the PU material. In contrast, a second transition that is found above room temperature can be associated to the disordering of the HS. This transition is of fundamental importance for the mechanical consistency of the material at room temperature. Due to the fact that the silica filler can be considered as an additional HS phase [28], the DMA analysis will focus on this transition.

The DMA analysis, represented by the Shear Storage Modulus (G') and the tan δ (damping factor) as a function of temperature are shown in Fig. 7. The behavior of the Neat-PU, the Sil-PU 3 wt%, and the Sil(16.7%)-PU 3 wt% are depicted. The Neat-PU was characterized by a G' of 616±11 MPa (at 30°C) which decreased by two orders of magnitude when the temperature reached values higher than 80°C. As far as the damping factor is concerned, a maximum was centered at 68°C with a value of 0.97. This dynamic transition was associated to the disordering of the HS [59]. This result is in agreement with the work of several authors [62–64]. As far as the behavior of the Sil-PU 3 wt% is concerned, the G' at 30°C was 655±9 MPa (slightly higher to the Neat-PU). In addition, the damping factor had a maximum value of 0.67, and it was centered at a temperature of 63±4°C. In contrast to the Neat-PU, the transition covered a much wider temperature range. Even at temperatures of around 40°C, a significant decrease of the G' was measured (−19%). As

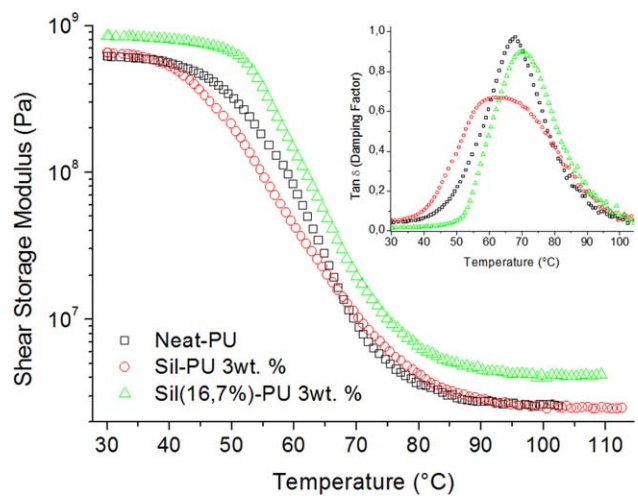

FIG. 7. Storage Shear Modulus as a function of temperature for the Neat-PU, the Sil-PU 3 wt %, and the Sil(16.7%)-PU 3 wt%. The inset shows the damping factor as a function of temperature for the same formulations. [Color figure can be viewed in the online issue, which is available at wileyonlinelibrary.com.]

far as the behavior of the Sil(16.7%)-PU 3 wt% is concerned, the G' at 30°C was 849±8 MPa. It represented an improvement of ~38% with respect to the Neat-PU. In addition, the damping factor had a maximum value of 0.90 and it was centered at a temperature of 70°C. In contrast to the Sil-PU 3 wt% and the Neat-PU, the G' did not decrease significantly up to temperatures of around 50°C.

The DMA analysis of the nanocomposites as a function of w_{of} is depicted in Fig. 8. In this case, the filler concentration was fixed at 3 wt%. At any temperature, the G' had a monotonous decrease as a function of increasing w_{of}. Specifically, the G' at 30°C decreased from 849±8 MPa to about 501±9 MPa for w_{of} values of 16.7 and 46.2%, respectively. In addition, the maximum of the damping factor was also shifted to lower temperatures as a function of increasing w_{of}. It should be noticed that these results were expected. If the nanoparticle had an elevated w_{of}, then, it is logical to assume that the properties of the PCL layer will prevail over the properties of the Silica core.

The DMA analysis as a function of filler concentration is shown in Fig. 9. The upper graph of Fig. 9 compares the behavior of a Sil(13.2%)-PU 0.5 wt%, a Sil(12.9%)-PU 1 wt%, and a Sil(16.7)-PU 3 wt%. Taking into account that the w_{of} were similar, then, it can be considered that the behavior was modified mainly by the filler concentration. An increase in concentration was followed by a monotonous increase of G', going from 629±12 MPa up to 849±8 MPa when the concentration increased from 0.5 to 3 wt%. The damping factor (reported in Table 2) did not show any significant change. It should be noticed that these results follow what it should be theoretically expected. In contrast, the lower graph of Fig. 9

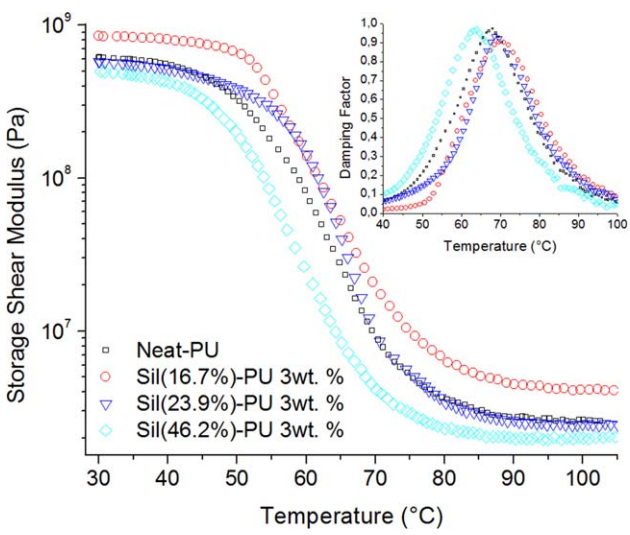

FIG. 8. Storage Shear Modulus as a function of Temperature for the Neat-PU, the Sil(16.7%)-PU 3 wt%, the Sil(23.9%)-PU 3 wt%, and the Sil(46.2%)-PU 3 wt%. The inset shows the damping factor as a function of temperature for the same formulations. [Color figure can be viewed in the online issue, which is available at wileyonlinelibrary.com.]

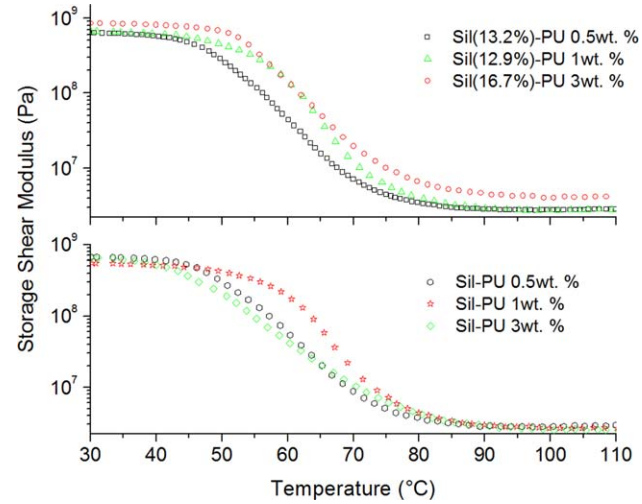

FIG. 9. Storage Shear Modulus (G') as a function of Temperature. The upper graph shows the behavior for the Sil(13.2%)-PU 0.5 wt%, the Sil(12.9%)-PU 1 wt%, and the Sil(16.7%)-PU 3 wt% nanocomposites. The lower graph shows the behavior of the Sil-PU at 0.5, 1, and 3 wt %. [Color figure can be viewed in the online issue, which is available at wileyonlinelibrary.com.]

compared the Sil-PU 0.5 wt%, the Sil-PU 1 wt%, and the Sil-PU 3 wt%. The G' did not follow a monotonous increase as a function of concentration. In fact, it is important to notice that the evolution of G' as a function of temperature for the Sil-PU 0.5 wt% and the Sil-PU 3 wt% were similar. Instead, the decrease of G' as a function temperature for the Sil-PU 1 wt% was more pronounced. In fact, at a temperature of 65°C, the G' for the Sil-PU 1 wt% was substantially higher with respect to the Sil-PU 0.5 wt% and the Sil-PU 3 wt%. From a theoretical point of view, a monotonous increase of G' as a function of increasing concentrations should be expected. However, that hypothesis is not valid in this case because the silanols surface groups on the SN modified the index of the PU formulation. Taking into account that the density of silanols [43] was 60×10^{-3} gOH.(gSiO_2)$^{-1}$, then, it can be calculated that the nanocomposites prepared at 0.5, 1, and 3 wt% increased the index by 0.58, 1.2, and 3.49%, respectively. It should be noticed that an increase of the index would cause a softer nanocomposite. Then, the SN-based nanocomposites were, from one side, reinforced by the mere presence of the filler but, from the other side, softened by the silanol groups of the SN. This

TABLE 2. Summary of DMA properties for the tested formulations.

	$G'_{30°C}$ (MPa)	$T_{(Tan\ d)}$ (°C)	|Tan δ|
Neat-PU	616±11	68±4,3	0.97
Sil-PU 1% wt	555±10	71±2	0.94
Sil-PU 3% wt	655±9	63±4	0.67
Sil(16,7)-PU 3% wt	849±8	70±3	0.9
Sil(23,9)-PU 3% wt	581±9	69±3	0.93
Sil(46,2)-PU 3% wt	501±7	63±5	0.97
Sil(12,9)-PU 1% wt	612±12	69±5	0.93

 DOI 10.1002/pen

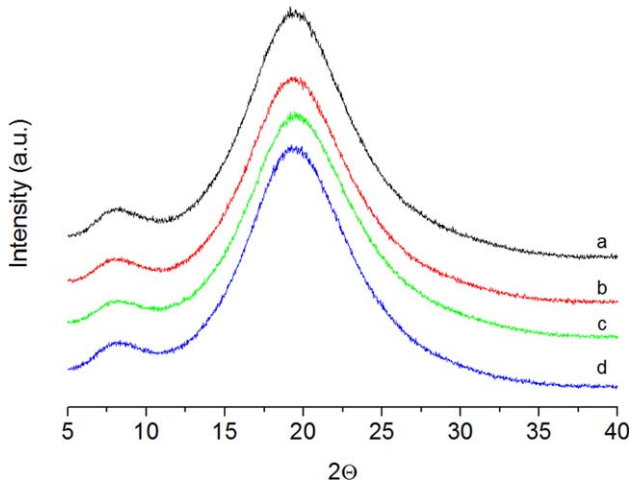

FIG. 10. WAXD patterns of (a) Neat-PU, (b) Sil-PU 1 wt %, (c) Sil-PU 3 wt%, and (d) Sil(12.9%)-PU 1 wt%. [Color figure can be viewed in the online issue, which is available at wileyonlinelibrary.com.]

twofold effect was not measured on the GN-based nanocomposites because the surface density of silanols was negligible.

Wide-angle X-Ray Diffraction of the Nanocomposites

The wide-angle X-ray diffraction (WAXD) patterns of the Neat-PU, the Sil-PU 1 wt%, the Sil-PU 3 wt%, and the Sil(12.9%)-PU 1 wt% are depicted in Fig. 10. Two broad peaks centered at $2\Theta = 8.4°$ and $2\Theta = 19.4°$ were found. Hence, it can be inferred that both the Neat-PU and the nanocomposites had some degree of crystallinity. Following what has been found by Trovati et al. [65], those peaks can be associated to the ordering of the HS and SS, respectively. It should be noticed that it is not the objective of this work to obtain the crystalline index of the samples but, rather, to compare the crystalline degree among the evaluated samples. For details about the crystalline index of nanocomposites similar to the ones studied in this work, the reader should consult Nunes et al. [61] or Saiani et al. [56–58]. The methodology used in this work to compare the relative variation of crystallinity is based on the work of Trovati et al. [65]. The degree of crystallinity was evaluated from the WAXD patterns using the Peak Fitting Module of a commercial software (Microlocal OriginLab 8.0). Then, by evaluating the area ratio of both peaks ($A_r = A_1/A_2$), a comparative degree of crystallinity among each sample can be obtained. The A_1 corresponded to the peak centered at $2\Theta = 8.4°$ while the A_2 corresponded to the peak centered at $2\Theta = 19.4°$. Hence, it can be inferred that an increasing A_r value would imply a more ordered HS structure. The calculated A_r values were 5.18, 4.8, 4.3, and 4.93, for the Neat-PU, the Sil-PU 1 wt%, the Sil-PU 3 wt%, and the Sil(12.9%)-PU 1 wt%, respectively. The first conclusion that can be obtained from those values is that the SN decreased the HS crystallinity. In fact, the A_r decreased monotonically as a function of increasing SN concentration. Instead, it can also be deduced that the GN improved the HS crystallinity. It should be noticed that this deduction is in agreement with both the DSC and DMA results previously exposed. As an example, the DSC results had shown that the GN particles increased the enthalpic energy associated to the transition of the HS. This result is corroborated by the WAXD experiments, where a higher order of crystallinity was also calculated.

CONCLUSIONS

The plausibility of implementing an environmentally friendly compatibilization process for the reinforcement of PU composites was evaluated. It was found that a simple and innocuous grafting process was able to conform core–shell SNs which contained organic weight fractions in the range 0–46%. The insertion of those GNs in a PU matrix has shown to produce a nanocomposite with improved mechanical properties, such as modulus and damping capacity. The grafting process improved the interfacial area between the matrix and the filler by the breakdown of the original silica agglomerates. In contrast to the SN, the GN-based nanocomposites achieved an improvement of elastic modulus and a nondetrimental effect on the HS transition temperature. The underlying phenomena which were responsible for those improvements were related to the fact that the GN filler improved the physical crosslinking among the HS. Instead, the SN had the opposite effect. Finally, the GN-based nanocomposites had an improved thermal stability in comparison with the SN nanocomposites, which offered no improvement whatsoever.

ACKNOWLEDGMENT

The authors acknowledge Ivan Barozzi and Valentina Tumidei from Neuchem S.R.L. and Chimicafine S.R.L. for providing the Albodur Polyol and the Isocyanate chemicals.

REFERENCES

1. F. Shao-Yun, F. Xi-Qiao, L. Bernd, and M. Yiu-Wing, *Compos. B: Eng.*, **39**, 933 (2008).
2. F. Hussain, M. Hojjati, M. Okamoto, and R.E. Gorga, *J Compos Mater.*, **40**, 1511 (2006).
3. Y.C. Ke and P. Stroeve, Polymer-Layered Silicate and Silica Nanocomposites, Elsevier Science, Amsterdam, The Netherlands, 2005.
4. R.N. Rothon, Particulate-filled polymer composites, Ed. Rapra Technologies, Shrewsbury, UK, 2003.
5. Y.R. Lee, A.V. Raghu, H.M. Jeong, and B.K. Kim, *Macromol. Chem. Phys.*, **210**, 1247 (2009).
6. D.A. Nguyen, Y.R. Lee, A.V. Raghu, H.M. Jeong, C.M. Shin, and B.K. Kim, *Polym. Int.*, **58**, 412 (2009).
7. A.V. Raghu, Y.R. Lee, H.M. Jeong, and C.M. Shin, *Macromol. Chem. Phys.*, **209**, 2487 (2008).
8. H. Zou, S.S. Wu, and J. Shen, *Chem. Rev.*, **108**, 3893 (2008).
9. G. Carrot, Rutot-D. Houze, A. Pottier, P. Degee, J. Hilborn, and P. Dubois, *Macromolecules*, **35**, 8400 (2002).

10. J. Casas, P.V. Persson, T. Iversen, and A. Córdova, *Adv. Synth. Catal.*, **346**, 1087 (2004).
11. B. Radhakrishnan, R. Ranjan, and W.J. Brittain, *Soft Matter.*, **2**, 386 (2006).
12. Y. Shin, D. Lee, K. Lee, K.H. Ahn, and B. Kim, *J. Ind. Eng. Chem.*, **14**, 515 (2008).
13. C. Dubois, M. Rajabian, and D. Rodrigue, *Polym. Eng. Sci.*, **46**, 360 (2006).
14. M. Joubert, C. Delaite, Bourgeat-E. Lami, and P. Dumas, *J. Polym. Sci. Polym. Chem.*, **42**, 1976 (2004).
15. M.K. Kiesewetter, E.J. Shin, J.L. Hedrick, and R.M. Waymouth, *Macromolecules*, **43**, 2093 (2010).
16. S. Benli, Ü. Yilmazer, F. Pekel, and S. Özkar, *J. Appl. Polym. Sci.*, **68**, 1057 (1998).
17. G.D. Chen, S.X. Zhou, H.M. Liao, and L.M. Wu, *J Compos Mater.*, **39**, 215 (2005).
18. T.G. Maciá-Agulló, J.C. Fernández-García, A. Torró-Palau, A.C. Orgilés Barceló, and J.M. Martín-Martínez, *J. Adhes.*, **50**, 265 (1995).
19. A.M. Torro-Palau, J.C. Fernandez-Garcia, A.C. Orgiles-Barcelo, and J.M. Martin-Martinez, *Int J. Adhes. Adhes.*, **21**, 1 (2001).
20. M. Joubert, C. Delaite, E.B. Lami, and P. Dumas, *New J. Chem.*, **29**, 1601 (2005).
21. S. Chen, J. Sui, and L. Chen, *Colloid Polym. Sci.*, **283**, 66 (2004).
22. X.C. Chen, L.M. Wu, S.X. Zhou, and B. You, *Polym. Int.*, **52**, 993 (2003).
23. X.C. Chen, B. You, S.X. Zhou, and L.M. Wu, *Surf. Interface Anal.*, **35**, 369 (2003).
24. Y.C. Chen, S.X. Zhou, H.H. Yang, and L.M. Wu, *J. Appl. Polym. Sci.*, **95**, 1032 (2005).
25. Z. Hosgor, Kayaman-N. Apohan, S. Karatas, Y. Menceloglu, and A. Gungor, *Prog. Org. Coat.*, **69**, 366 (2010).
26. S. Kang, S.I. Hong, C.R. Choe, M. Park, S. Rim, and J. Kim, *Polymer*, **42**, 879 (2001).
27. B.S. Kim, S.H. Park, and B.K. Kim, *Colloid Polym. Sci.*, **284**, 1067 (2006).
28. Z.S. Petrović, Y.J. Cho, I. Javni, S. Magonov, N. Yerina, D.W. Schaefer, J. Ilavský, A. Waddon, *Polymer*, **45**, 4285 (2004).
29. L. Indennidate, D. Cannoletta, F. Lionetto, A. Greco, and A. Maffezzoli, *Polym. Int.*, **59**, 486 (2010).
30. F. Lionetto, L. Mascia, and M. Frigione, *Eur. Polym. J.*, **49**, 1298 (2013).
31. F. Lionetto and A. Maffezzoli, *Appl. Rheol.*, **19**:23423–23431.
32. Z.S. Petrovic, I. Javni, A. Waddon, and G. Banhegyi, *J. Appl. Polym. Sci.*, 2000;**76**, 133 (2009).
33. S.I. Lee, Y.B. Hahn, K.S. Nahm, and Y.S. Lee, *Polym. Adv. Technol.*, **16**, 328 (2005).
34. M.I. Aranguren, N.E. Marcovich, W. Salgueiro, and A. Somoza, *Polym. Test.*, **32**, 115 (2013).
35. R.V. Silva, D. Spinelli, W. Bose,W. Filho, S. Claro, Neto, G.O. Chierice, and J.R. Tarpani, *Compos. Sci. Technol.*, **66**, 1328 (2006).
36. S. Chen, Q. Wang, and T. Wang, *Mater Chem. Phys.*, **130**, 680 (2011).
37. A.J. Varma, M.D. Deshpande, and V.M. Nadkarni, *Die Angew. Makromol. Chem.*, **132**, 203 (1985).
38. Y. Xia and R.C. Larock, *Macromol. Rapid Commun.*, **32**, 1331 (2011).
39. A. Kaushik, D. Ahuja, and V. Salwani, *Compos. A: Appl. Sci. Manufact.*, **42**, 1534 (2011).
40. C. Merlini, V. Soldi, and G.M.O. Barra, *Polym. Test.*, **30**, 833 (2011).
41. J. Fiorelli, D.D. Curtolo, N.G. Barrero, H. Savastano Jr., E.M. de Jesus Agnolon Pallone, and R. Johnson, *Ind. Crops Prod.*, **40**, 69 (2012).
42. I.S. Ristić, J. Budinski-Simendić, I. Krakovsky, H. Valentova, R. Radičević, S. Cakić, N. Nikolić, *Mater. Chem.Phys.*, **132**, 74 (2012).
43. R. Bode, H. Ferch, *H.F. Degussa AG.*, 2006.
44. J.H. Moon, B. Ramaraj, S.M. Lee, and K.R. Yoon, *J. Appl. Polym. Sci.*, **107**, 2689 (2008).
45. E. Oledzka and S.S. Narine, *J. Appl. Polym. Sci.*, **119**, 1873 (2011).
46. J. Kadota, Pavlović D., J.-P. Desvergne, B. Bibal, F. Peruch, and A. *Deffieux, Macromolecules*, **43**, 8874 (2010).
47. Available at wwwvma-getzmanncom. Downloaded 21/12/2011.
48. A.V. Raghu, G.S. Gadaginamath, H.M. Jeong, N.T. Mathew, S.B. Halligudi, and T.M. Aminabhavi, *J. Appl. Polym. Sci.*, **113**, 2747 (2009).
49. A.V. Raghu and H.M. Jeong, *J. Appl. Polym. Sci.*, **107**, 3401 (2008).
50. S.X. Zhou, L.M. Wu, J. Sun, and W.D. Shen, *Prog. Org. Coat.*, **45**, 33 (2002).
51. S.X. Zhou, L.M. Wu, J. Sun, and W.D. Shen, *J. Appl. Polym. Sci.*, **88**, 189 (2003).
52. M.A. Corcuera, L. Rueda, B. Fernandez d'Arlas, A. Arbelaiz, C. Marieta, I. Mondragon, A. Eceiza *Polym. Degrad.Stab.*, **95**, 2175 (2010).
53. Ivan S. Ristić, Zoran D. Bjelović, Berta Holló, Katalin Mészáros Szécsényi, Jaroslava Budinski-Simendić, Nada Lazić, Miodrag Kićanović, *J. Therm. Anal. Calorim.*, **111**, 1083 (2013).
54. I. Javni, Z.S. Petrović, A. Guo, R. Fuller, *J. Appl. Polym. Sci.*, **77**, 1723 (2000).
55. C. Prisacariu, *Springer Vienna.*, 2011.
56. A. Saiani, A. Novak, L. Rodier, G. Eeckhaut, J.W. Leenslag, J.S. Higgins, *Macromolecules*, **40**, 7252 (2007).
57. A. Saiani, W.A. Daunch, H. Verbeke, J.W. Leenslag, J.S. Higgins, *Macromolecules*, **34**, 9059 (2001).
58. A. Saiani, C. Rochas, G. Eeckhaut, W.A. Daunch, J.W. Leenslag, J.S. Higgins, *Macromolecules*, **37**, 1411 (2004).
59. D. Randall, S. Lee, *Wiley*, 2003.
60. M. Szycher, CRC *Press* LLC, New York, USA. 1999.
61. R.C.R. Nunes, R.A. Pereira, J.L.C. Fonseca, and M.R. Pereira, *Polym. Test.*, **20**, 707 (2001).
62. G. Gorrasi, M. Tortora, and V. Vittoria, *J. Polym. Sci. Part B: Polym. Phys.*, **43**, 2454 (2005).
63. M. Tortora, G. Gorrasi, V. Vittoria, G. Galli, S. Ritrovati, and E. Chiellini, *Polymer*, **43**, 6147 (2002).
64. M. Tortora, V. Vittoria, G. Galli, S. Ritrovati, and E. Chiellini, *Macromol. Mater. Eng.*, **287**, 243 (2002).
65. G. Trovati, E.A. Sanches, S.C. Neto, Y.P. Mascarenhas, and G.O. Chierice, *J. Appl. Polym. Sci.*, **115**, 263 (2010).